Geophysical Research Letters

RESEARCH LETTER
10.1029/2020GL090244

Special Section:
The Covid-19 Pandemic: Linking Health, Society and Environment

Local Anomalies in the Column-Averaged Dry Air Mole Fractions of Carbon Dioxide Across the Globe During the First Months of the Coronavirus Recession

Frédéric Chevallier[1], Bo Zheng[1], Grégoire Broquet[1], Philippe Ciais[1], Zhu Liu[2], Steven J. Davis[3], Zhu Deng[2], Yilong Wang[4], François-Marie Bréon[1], and Christopher W. O'Dell[5]

[1]Laboratoire des Sciences du Climat et de l'Environnement, LSCE/IPSL, CEA-CNRS-UVSQ, Université Paris-Saclay, Gif-sur-Yvette, France, [2]Department of Earth System Science, Tsinghua University, Beijing, China, [3]Department of Earth System Science, University of California, Irvine, CA, USA, [4]Key Laboratory of Land Surface Pattern and Simulation, Institute of Geographical Sciences and Natural Resources Research, Chinese Academy of Sciences, Beijing, China, [5]Cooperative Institute for Research in the Atmosphere, Colorado State University, Fort Collins, CO, USA

Key Points:
- Covid-19 impacted the CO_2 column mostly in the vicinity of a few emission locations that changed over time
- These places have not been well observed by the OCO-2 satellite because of frequent or persistent cloud conditions
- To support the Paris Agreement on climate, priority should be given on the development of all-weather carbon-monitoring systems

Supporting Information:
- Supporting Information S1

Correspondence to:
F. Chevallier,
frederic.chevallier@lsce.ipsl.fr

Citation:
Chevallier, F., Zheng, B., Broquet, G., Ciais, P., Liu, Z., Davis, S. J., et al. (2020). Local anomalies in the column-averaged dry air mole fractions of carbon dioxide across the globe during the first months of the coronavirus recession. *Geophysical Research Letters*, *47*, e2020GL090244. https://doi.org/10.1029/2020GL090244

Received 11 AUG 2020
Accepted 21 OCT 2020
Accepted article online 29 OCT 2020

Abstract We use a global transport model and satellite retrievals of the carbon dioxide (CO_2) column average to explore the impact of CO_2 emissions reductions that occurred during the economic downturn at the start of the Covid-19 pandemic. The changes in the column averages are substantial in a few places of the model global grid, but the induced gradients are most often less than the random errors of the retrievals. The current necessity to restrict the quality-assured column retrievals to almost cloud-free areas appears to be a major obstacle in identifying changes in CO_2 emissions. Indeed, large changes have occurred in the presence of clouds, and in places that were cloud free in 2020, the comparison with previous years is hampered by different cloud conditions during these years. We therefore recommend to favor all-weather CO_2 monitoring systems, at least in situ, to support international efforts to reduce emissions.

Plain Language Summary The first half of 2020 represents an extreme period for the global carbon cycle with both exceptionally low carbon dioxide emissions from the use of fossil fuels and exceptionally high temperatures around the world. Here, we study the changes in human emissions witnessed from space by NASA's second Orbiting Carbon Observatory (OCO-2) from February to May 2020. We then reassess user needs for future carbon-dioxide observing systems that will monitor human emissions.

1. Introduction

The coronavirus disease 2019 (Covid-19) has severely disrupted the global economy by collapsing travel, the production of goods, and the demand for goods at the same time, in an unprecedented way. Subsequent reductions in CO_2 emissions associated with the use of fossil fuels have received particular attention in the context of the ambitious emission reduction targets implied by the 2015 International Paris Agreement (PA) on climate: typical pathways limiting global warming to 1.5°C reduce global emission by 3–4% per year for several decades from now on (IPCC, 2018). Indicators of industrial activity and data on fossil fuel consumption made it possible to very quickly estimate the significant drop in CO_2 emissions that was occurring in China (Myllyvirta, 2020). Weeks later, estimates for the whole globe indicated that the reduction from the same months in 2019 temporarily reached around 20%, bringing the global emission level in the beginning of April back 14 years to the past, in 2006 (Tollefson, 2020). From a methodological point of view, these estimates are often said to be "bottom-up" because they are based on data related to the causes of changes in emissions. In their own formal framework, national emissions reports submitted to the United Nations Framework Convention on Climate Change (UNFCCC) are essentially of the same nature (IPCC, 2006).

Bottom-up estimates suffer from various limitations in terms of objectivity, completeness, and modeling assumptions, and major international efforts are underway to support the development of greenhouse gas inventories using atmospheric measurements. Atmospheric measurements are the basis for "top-down" emission estimates, that is, based on the observed effects of these emission changes into the atmosphere. On a large scale, to our knowledge, no top-down estimate of Covid-19 emission reductions has been provided using direct observations of CO_2, either in situ or from space. This gap is easily explained by the focus of most

existing large-scale CO_2 observing systems on the natural component of the carbon cycle rather than on its anthropogenic component, a situation which will soon evolve: by the end of the decade, CO_2 observing systems dedicated to monitoring anthropogenic emissions will be deployed (Janssens-Maenhout et al., 2020). However, the main difference between existing and future systems is not yet about disruptive innovations in measurement techniques, but rather about sampling density: the introduction of large-scale satellite imagery of CO_2 and the expansion of in situ urban CO_2 networks, including isotopes and other additional tracers. In addition, the new systems will be used to quantify emission reduction signals that will not be larger than the ones induced by Covid-19 in the first half of 2020 (~20%; Le Quéré et al., 2020). Country-wide changes in 5-year intervals between two emissions censuses of the PA (Pinty et al., 2017) will at best share the same order of magnitude as the 14-year-equivalent pulse signal triggered by Covid-19 worldwide.

Here, we study the changes in the column-average dry air-mole fraction of CO_2 (XCO_2) retrieved from the second Orbiting Carbon Observatory (OCO-2) during the first months of the coronavirus recession, from February to May 2020. After the presentation of our data and the methods in section 2, section 3 begins with a global simulation of the transport of CO_2 in the atmosphere which allows us to estimate the order of magnitude and the location of the Covid-19-induced XCO_2 signal. It then focusses on the local enhancements in the XCO_2 retrieved for the first few months of the year over the 6 years of OCO-2 observations. General conclusions are drawn in section 4.

2. Data and Methods

2.1. Satellite Retrievals

This study uses the XCO_2 retrievals from the OCO-2 satellite (Eldering et al., 2017). Since the start of its science operations in the summer of 2014, OCO-2 has been orbiting from pole to pole with a 16-day repeat cycle and a local passage at the equator around 1:30 p.m. when traveling from south to north. Its spectrometer measures sunlight reflected from the Earth and its atmosphere in the near infrared/short-wave infrared spectral regions with an individual surface footprint of only a few km^2. Above the sunlit hemisphere, the instrument is oriented either directly down to the local nadir or toward the specular solar direction, except for specific target observations. Radiance measurements along the orbit track are returned as eight spots across a swath of approximately 10 km. Under sufficiently cloud and aerosol-free conditions, each of the measurement points can be analyzed to retrieve XCO_2. We use version 10 of the official XCO_2 retrievals over both land (glint or nadir pointing modes) and ocean made by the NASA Atmospheric CO_2 Observations from Space (ACOS) algorithm described by Osterman et al. (2020). This algorithm follows both a Bayesian estimation procedure, including a detailed radiation model, and an empirical parametric bias correction.

Our study focuses on XCO_2 enhancements along the OCO-2 orbit tracks that are caused by fossil fuel emissions. This focus leads us to select the vicinity of the combustion sources using the collocated nitrogen dioxide (NO_2) tropospheric vertical column density (TCVD) retrievals from the Ozone Monitoring Instrument (OMI; Levelt et al., 2006) on board the Aura spacecraft of NASA. NO_2 is emitted by the same combustion processes as CO_2, but with a short lifetime in the atmosphere (a few hours in the boundary layer during the day). The OMI archive started in 2004 and is still ongoing. It therefore covers the complete record of the OCO-2 instrument. Aura flies near OCO-2 within the Afternoon Train (A-train) constellation: its local equator crossing time is 1:45 p.m. on the ascending node. OMI is a near UV/visible spectrometer with a much coarser spatial resolution than OCO-2 (13×24 km^2 ground pixels at nadir), but with a much larger swath (2,600 km) which allows coverage of most of the globe in 1 day. The quality of the retrievals is also less sensitive to clouds, so the clouds are less filtered than for the OCO-2 retrievals. Version 3.0 of the standard OMI product is used here (Krotkov et al., 2017). In this study, individual OMI retrievals with good quality ($VcdQualityFlags = 0$) were pre-averaged at a global resolution of 0.5° and daily.

To map bottom-up fossil fuel CO_2 emissions at the scale of a country on a regular grid to do CO_2 transport modeling, we use another NO_2 TCVD retrieval product from the Tropospheric Monitoring Instrument (TROPOMI) on board the Sentinel-5 Precursor satellite, launched in October 2017 (Veefkind et al., 2012). TROPOMI NO_2 retrievals have much higher spatial resolution than OMI, while keeping the same swath width (2,600 km): the ground resolution of the retrievals was 7×3.5 km^2 at nadir until 5 August 2019 and has been 5.5×3.5 km^2 afterwards. Standard retrievals from the official offline processing (van Geffen

et al., 2019) with a quality assurance value greater than 0.75 were aggregated here daily on a regular 0.1° × 0.1° global grid and averaged over running 15-day periods in order to dampen the retrieval noise and reduce gaps in the maps. The 0.1° resolution allowed by the high resolution of TROPOMI describes changes in NO_2 TCVD across country borders or model grid boxes much better than the 0.5° grid that we use with OMI.

2.2. From Local XCO_2 Enhancements to Local Emission Estimates

After the first work of Nassar et al. (2017) and Reuter et al. (2019), Zheng, Chevallier, et al. (2020) developed a method to estimate the emissions that are associated with atmospheric plumes from isolated clusters of anthropogenic CO_2 emissions (cities and industrial areas) that are visible in OCO-2 retrievals over China. We have adapted the initial algorithm to the whole world in order to fully automate the procedure and remove the specificities for China. The modified algorithm works as follows.

Each OCO-2 retrieval is analyzed in the context of the 200-km orbit segment that surrounds it, i.e., the ensemble of retrievals that are less than 100 km away from it. Only good-quality bias-corrected retrievals are taken into account (*xco2_quality_flag* = 0), and only soundings belonging to the same surface type (terrestrial or oceanic) are compared together. Retrievals that differ from the segment median (for the same surface type) by more than twice the standard deviation are reported as possibly on the ridge of a plume.

For each flagged sounding, a second step attempts at fitting a function of the distance along the satellite track on the XCO_2 retrievals of the same surface type in this segment, accounting for the relative uncertainty of each sounding (as defined by the variable *xco2_uncertainty*). The function represents an isolated local plume on a background level produced from sources and sinks from the rest of the world. It has four parameters. The first two parameters are the slope and the offset of an XCO_2 background that is linear along the track distance. The other two parameters are the standard deviation s and the amplitude a of a Gaussian function centered on the flagged retrieval and varying with the distance along the trajectory of the orbit. The resulting fit is evaluated on the basis of several criteria: s must be between 2.5 and 30 km; a must be greater than the XCO_2 standard deviation on the segment; in order to avoid significant data gaps, there must be at least one valid XCO_2 retrieval per km, on average on each side of the peak for along-track distances less than s or between $2 \times s$ and $3 \times s$; the coefficient of determination (r^2) of the Gaussian adjustment must be greater than 0.4. Since the procedure is based on a 200-km rolling segment, neighboring Gaussians may actually describe the same enhancement: when the peaks of two Gaussian fits are within $2 \times s$ of each other (with s successively taking the values of both fits), only the fit with the largest r^2 is kept.

A third step limits the cases to the vicinity of the fossil fuel emission zones. Zheng, Chevallier, et al. (2020) used a detailed inventory of China for this. We have replaced this with a simple threshold on NO_2 TCVD retrieved from OMI: cases are kept if the maximum gridded TCVD between the day before and the next day (3 values, in order to compensate for the incomplete global coverage of the instrument each day) at the peak of the Gaussian curve is greater than 10^{15} molecules per cm^2.

The last step recovers the associated emission by multiplying the density of the plume along the track (given by the area under the Gaussian curve with the surface pressure and the total column water vapor) by the wind speed in the direction normal to the OCO-2 track. The wind speed here is the wind analyzed by the fifth generation of ECMWF atmospheric reanalyses of the global climate (ERA5; Hersbach et al., 2020) in the model second level from the surface (corresponding to a geometric altitude of about 31 m). Using higher levels increases the wind values and therefore the estimated emissions, but does not affect the relative changes in emissions presented in the following. The surface pressure is the a priori value used in the OCO-2 retrieval. The total column water vapor is the OCO-2 value retrieved together with XCO_2. This step provides a collection of local emission estimates around noon or in the late morning.

2.3. Global Model Simulation

Our simulation of CO_2 transport in the global atmosphere is based on the general circulation model of the Laboratoire de Météorologie Dynamique (LMDz; Hourdin et al., 2013) nudged toward horizontal winds analyzed by ERA5. More precisely, we use the LMDz6A version, discussed by Remaud et al. (2018) for the transport of tracers, with 39 hybrid layers in the vertical and a regular horizontal resolution of 3.75° in longitude and 1.875° in latitude.

Hereinafter, we call $FFCO_2$ the CO_2 emissions from the use of fossil fuels and the production of cement. We use LMDz to propagate the impact of the difference in $FFCO_2$ between the years 2019 and 2020 with the meteorology of 2020. The difference is defined as the 2020 emissions minus 2019, an amount that is generally, but not always, negative for the months studied here. The simulation begins on 1 January 2020 at 00:00 UTC from a CO_2-free atmosphere and ends on 31 May 2020 at 24:00 UTC after being forced by no other surface flux than the difference in $FFCO_2$. These emissions are those estimated by the Carbonmonitor project (Carbonmonitor, 2020; Liu et al., 2020) from a bottom-up perspective. Carbonmonitor documents daily emissions for 2019 and 2020 in a series of countries or groups of countries: Brazil, China, the 27-member European Union and United Kingdom together, France, Germany, India, Italy, Japan, Russia, Spain, the United Kingdom, the United States, and the rest of the world. For the first 5 months of 2020, the overall reduction in emissions reaches 336.4 Mt of carbon (C), which represents 8.6% of 2019 emissions for the same months. Almost half of the reduction comes from a drastic change in emissions from ground transport, while changes in emissions from power generation and industry only represent a quarter and a fifth of the reduction, respectively. The main countries contributing to the overall reduction are the United States (for 23% of the reduction, mainly after the end of March), China (for 18%, mainly in February and March), India (for 14%, mainly after end of March), and Germany (4.3%, mainly after end of March). The other countries contribute less than 3% to the reduction.

The Carbonmonitor numbers for the 11 countries reported and for EU28 (defined as the 27-member European Union and United Kingdom together) have been disaggregated on the LMDz horizontal grid with the following assumption: we assume that the spatial variation of the emission difference within a given country or group of countries follows the difference of 2020-minus-2019 NO_2 TCVDs of TROPOMI; we restrict the variations to the most polluted areas, defined as the 5% pixels with the largest TCVD on average between 1 January and 31 May 2019. Note that this procedure allows both increases and decreases in emissions if the sign of the retrieval difference changes for the same date in the same territory. Before disaggregation, Carbonmonitor's daily emissions are smoothed with 15-day running means, for consistency with our 15-day rolling average of the TROPOMI retrievals. The Carbonmonitor numbers for the "rest of the world," which represent 21% of the reduction in emissions, were not used because its surface area makes the local impact of its reduction in emissions marginal while reducing the significance of the 5% of the most polluted pixels for our disaggregation purpose. The daily Carbonmonitor numbers have not been disaggregated in time: we do not assume any diurnal cycle for the emissions.

3. Results

Figure 1 shows the largest negative values, per month, of the change in the global transport model XCO_2 around the OCO-2 passage time induced by the change of $FFCO_2$. All values are relative to the South Pole in order to focus on the spatial gradients rather than on the overall trend.

The Beijing Municipality and the neighboring provinces of eastern China are the only territories with a regional XCO_2 signal in February: up to -1 μmol mol^{-1} (micromole per mole, abbreviated as ppm, for parts per million, in what follows) on a monthly average and up to -2 ppm for instantaneous model values. In March, with the ease of restrictions in China, this signal gradually decreases (down to -0.5 ppm on average over the month alone), while depletions (compared to 2019 conditions) begin to be observed in the northeastern United States (down to -0.8 ppm around New York) and in central Siberia near the Beryozovskaya lignite power plant (down to -1.6 ppm for instantaneous US values, but without any significant monthly average). In April, Germany, Poland, the southwestern border of Russia, the United States around Seattle, Los Angeles, and Denver, and the northeastern corner of India are also depletion regions in the simulation of the model, with the same order of magnitude (a few tenths of ppm on average with sometimes 10 times higher instantaneous values). In May, most of the depletion occurs in the eastern United States and Europe, still with similar amplitudes.

We understand from Figure 1 that the impact of the emission reduction is mainly local and that a global transport model with a horizontal resolution of about 300 km, like the one used here, may isolate it easily (only $FFCO_2$ is transported here), but cannot quantify it accurately.

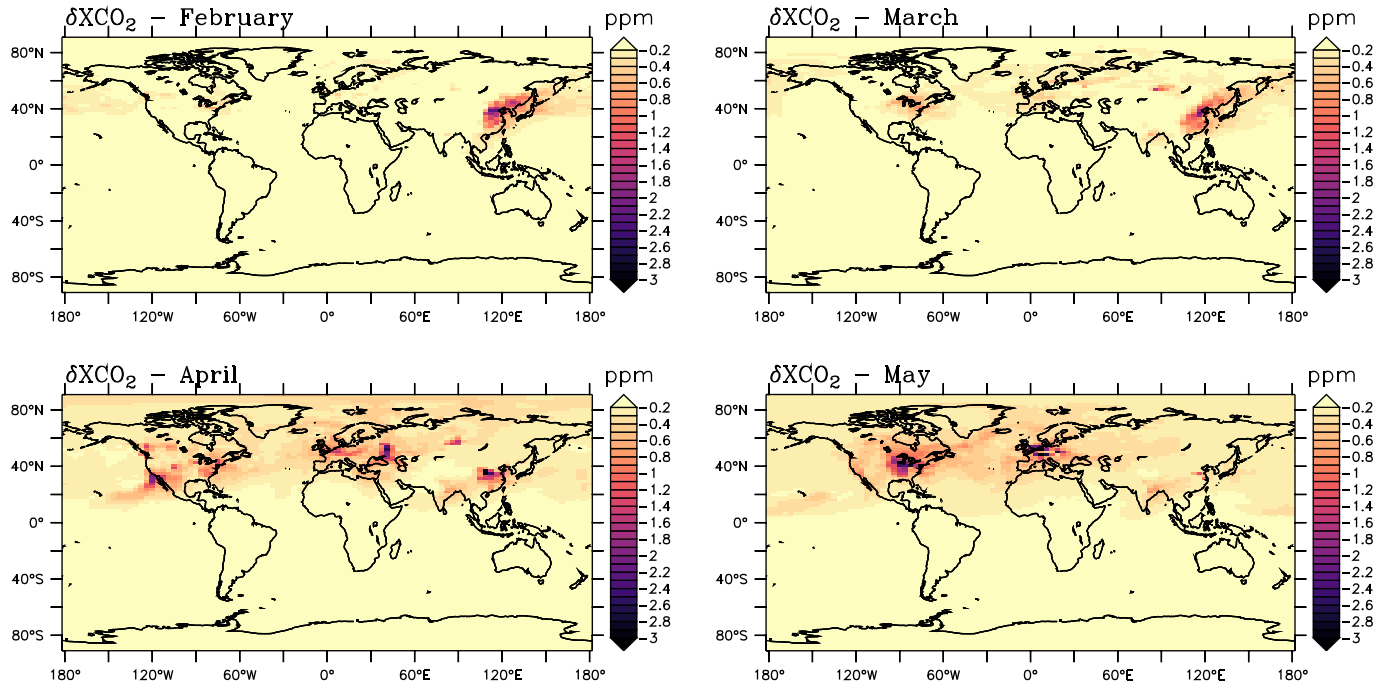

Figure 1. Monthly minimum gradients of δXCO_2(the perturbation induced by changes in $FFCO_2$between 2019 and 2020) relative to the South Pole simulated over the months of February, March, and April 2020 around local noon. They are all negative. The minimum value in the figure is −2.3, −2.2, −3.5, and −7.4 ppm in February, March, April, and May, respectively. Subtracting δXCO_2at South Pole removes the changes induced by the global growth rate.

We now try to zoom into the regions of interest with the OCO-2 XCO_2 retrievals that reach kilometer-scale resolution. A first basic requirement for this task is the acquisition of data on the few regions where the reduction signal manifested itself: eastern China, eastern United States and, to a lesser extent, the western coast of the United States, Europe, Western Russia, and some urban areas (Denver, Calcutta, and the Siberian power station). From an instrument like OCO-2, which observes the Earth with a swath of 10 km only, we do not expect dense local sampling, but examining the locations of the OCO-2 data shows additional complications. Low solar elevations reduce the signal and prevent the retrieval of XCO_2 in the mid to high latitudes of the winter hemisphere. In the case of the Covid-19 reduction of emissions, this could affect the observation of Europe, but the reduction signal in Europe starts late enough (April) to be observable by OCO-2 in principle. However, the dominance of cloudy conditions in China (see, e.g., the climatology of total visible cloud cover of Warren et al., 2015), systematically disrupts the retrieval of XCO_2 along satellite orbits and leaves much of this country unobserved for most of the study period, particularly around the Hubei province (Figure 2a). Around Beijing, only a few short segments of orbits with valid data points are available for each month, which makes it difficult to describe the XCO_2 emission plumes in their environment. Likewise, the lockdown in India began in late March, just before pre-monsoon conditions increased the appearance of cirrus clouds and gradually hampered the retrievals. In the United States, cloudless conditions are mainly observed in its western part, where only part of the relative depletion has occurred. By comparison, Carbonmonitor's estimates of daily emissions shows large variations from 1 week to the next, even for the “normal” year 2019.

With the global transport model, we could consider the signal from $FFCO_2$ change in isolation. In practice, this signal is superimposed on other changes in anthropogenic emissions (combustion of biofuels, human and animal respiration, managed ecosystems; see Ciais et al., 2020) and on changes in natural fluxes from the terrestrial biosphere and oceans. The plume analysis described in section 2 aims to select plumes from isolated emission clusters and remove the imprint of surface fluxes in their environment before estimating the emission from these isolated clusters. Strictly speaking, this distinction between what is inside a source cluster and what is outside imperfectly reflects the distinction between $FFCO_2$ and other surface fluxes. Nevertheless, we consider it a good approximation when studying a major change in $FFCO_2$.

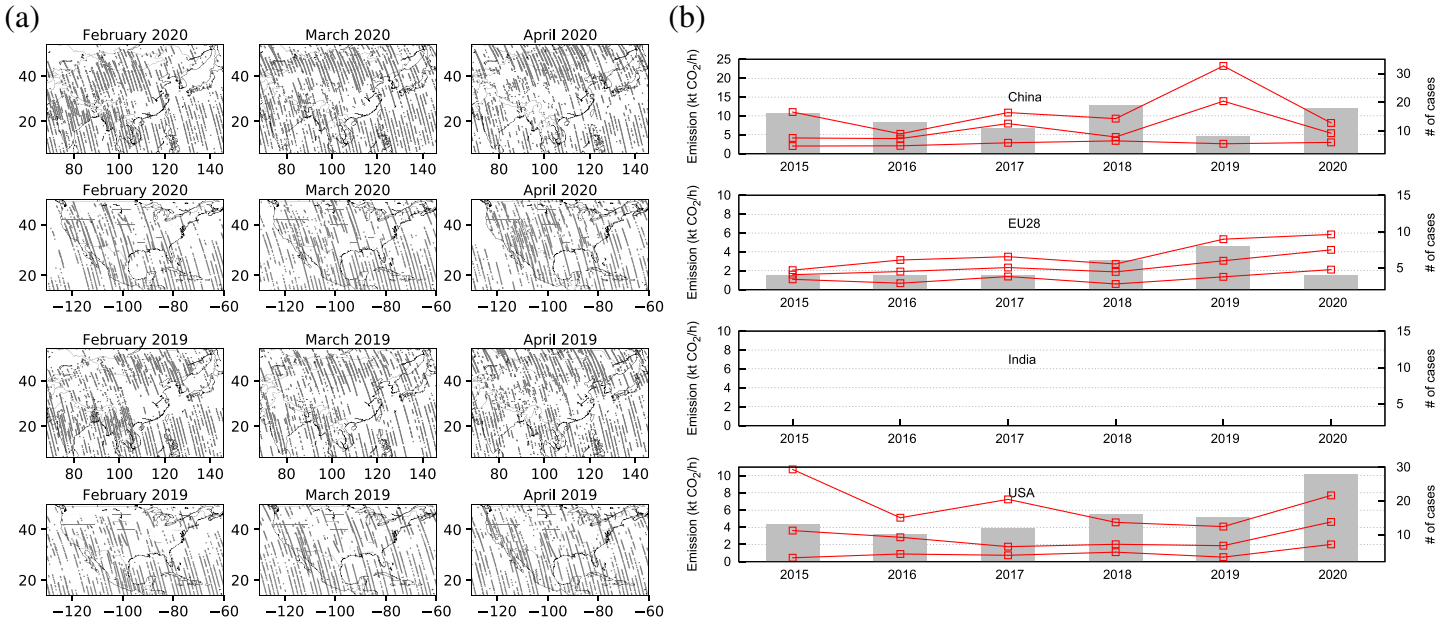

Figure 2. (a) location of "good-quality" OCO-2 XCO_2retrievals in Southeast Asia and in conterminous United States, Mexico, and some Central American countries during the months February, March, and April 2020 and 2019. (b) The three red lines are the time series of emission quartiles from individual emitting sources based on OCO-2 per year for February and March (China) or 20 March to 31 May (EU28, India, and United States). The gray boxes indicate the number of cases used in the statistics, with a minimum of 4 (which is never reached for India).

For the period between 1 February and 31 May 2020, the collection of analyzed plumes includes 902 cases over the globe. Corresponding amplitudes, a, of the Gaussian functions are between 0.4 and 6.1 ppm, with a mean of 1.8 ppm and a standard deviation of 0.9 ppm. In order to ease the interpretation, we gather them over each large emitting country (China, India, the United Staes) or group of countries (EU28) and discuss them in terms of estimated emissions. These four administrative territories represent between 14% (India) and 23% (United States) of the overall reduction in emissions estimated by Carbonmonitor. Together, they represent 72% of this quantity. The statistics are established for each year of OCO-2 operations over the period when the maximum impact of the quarantine measures is expected: February and March for China and the dates after 20 March (inclusive) for the other territories.

Figure 2b presents the quartiles of the emission estimates. The middle line is therefore the median. The first obvious feature is the lack (<4) of isolated plumes identified over India for all years (not just 2020) despite its large $FFCO_2$ emissions: Carbonmonitor estimates them to be close to that of the EU28 and half that of the United States in the first 5 months of 2019. This rarity is directly linked to the sparse retrieval density for these months, illustrated in Figure 2a. About 10 isolated local plumes are found each year before 20 March (not shown), but they are not interesting here.

For China, consistent with the orbit tracks shown in Figure 2a, most of the isolated plumes are found in the northern provinces: eight (six) cases in 2020 (2019) in Xinjiang, Inner Mongolia and Ninxia together. There are twice as many plumes across China in 2020 as in 2019, but actually, the number of cases in 2020 is the same as in 2018 and therefore cannot be considered extreme. In terms of emission levels, the 2020 statistics are within the statistics of the previous years. We note that the plumes were not sampled either in Hebei (the province surrounding the municipalities of Beijing and Tianjin) or in Liaoning (its neighboring northeastern province) in 2020, while some were identified in 2016 (three cases in the two provinces together), 2017 (four cases), 2018 (one case), and 2019 (two cases). The Beijing Municipality and the Tianjin Municipality did not appear in the plume results throughout the 5 years. However, the few orbit segments available each year over the area are not sufficient for a clear interpretation (see data coverage for 2019 in Figure 2a).

For the EU28, most of the plumes are observed in the western countries (France and the United Kingdom), the southwestern countries (Portugal, Spain, and Italy), and Austria. The plumes over the most emitting countries of central or eastern Europe may not be isolated enough to be selected by the algorithm. The

number of plumes identified is much lower in 2020 than in 2018 and 2019 but reaches the same value (4) as for the first 3 years of the satellite. The three quartiles are the largest in 2020 among the 6 years.

For the United States, nearly 30 plumes are identified in 2020, more than double from each previous year. The first quartile and the median are largest in 2020, but the third quartile was larger in 2015. The largest number of plumes is dominated by increases in the southwest: California (+3 vs. 2019), Nevada (+1), Utah (+1), Arizona (+2), and New Mexico (+4). This paradox of a greater plume count while the emissions were rather decreasing over the area (as confirmed, e.g., by comparing NO_2 TCVD retrievals from TROPOMI for 2019 and 2020), could simply be explained by the increased density of quality-assured XCO_2 retrievals in 2020 (see April data coverage in Figure 2a).

4. Conclusions and Discussion

In addition to the dramatic health and economic consequences it has worldwide, the Covid-19 pandemic offers unique opportunities to test the ability of the observing systems to document a major change in human behavior and in the environment. The variations in human CO_2 emissions have been considerable within just a few months, but, depending on both their human origin and the specific local development of the pandemic, have been concentrated in some places that changed over time. In early April, emissions in China rebounded to pre-pandemic levels (Zheng, Geng, et al., 2020) as several Western countries had only started restrictions on mobility. Within the same country, Covid-induced emission reductions could coexist with an increase in emissions linked or not to the pandemic: according to the National Bureau of Statistics of China (http://data.stats.gov.cn/english/), thermal power generation in some western provinces of China (Yunnan, Xinjiang, and Guangxi) notably increased in March, while it decreased in the eastern provinces of China. Local emission signals in a few places only generate local XCO_2 gradients in these same places because atmospheric diffusion rapidly disperses anthropogenic emission plumes (e.g., Broquet et al., 2018): gradients downstream the emission areas are usually not significant and are merged with other gradients induced by natural sources and sinks. It is therefore essential that any future observation-based CO_2 emissions monitoring system systematically acquires data at the specific locations where emissions variations occur.

The launch of CO_2 imagers (e.g., Clery, 2019) will address this issue, but our analysis of the OCO-2 quality-assured retrievals during the pandemic shows no clear sign of the 14-year-equivalent pulse signal triggered by Covid-19 on emissions worldwide. It evidences a limitation of current observing technology which is more fundamental than too short swath or an insufficient number of platforms to carry the instruments: OCO-2 measured the radiances over the main emission reduction areas, but persistent cloudy conditions at large scale often prevented the retrieval of quality-assured XCO_2, for example, in the province of Hubei in China, whose capital, Wuhan (11 million inhabitants) and neighboring towns were locked down at the end of January. This was also the case around Bengal when India was locked down. Variation in cloud conditions from year to year, for example, around Beijing or in the southwestern United States, also prevents the detection of changes. A constellation of identical OCO-2 instruments or an equivalent of OCO-2 with a large swath would not have changed this limitation much.

The user requirements defined for the future constellation of European CO_2 imagers place a threshold on XCO_2 systematic errors only for cloud cover less than 5% (ESA, 2019). We anticipate that this focus on near cloudless conditions is insufficient to make it the backbone of CO_2 emissions monitoring systems that would support the PA or provide robust metrics to a carbon market, because some of the target signals correlate with cloudiness: CO_2 emissions occurring under a cloud system may be different from emissions occurring in a clear sky at other locations or at the same location after the cloud system has disappeared, not only due to changes in home heating, but more generally because the timescale of cloudiness changes may correspond to the timescale of large changes in emissions. The very strict user requirements on XCO_2 retrievals systematic errors (e.g., Chevallier et al., 2005) have led to a restriction of these retrievals to very small amounts of clouds, but we suggest that this restriction is in turn incompatible with certain specific uses of the data. To support the PA, priority should be given on the development of all-weather CO_2 monitoring systems, ideally from space but at least in situ (e.g., Gurney et al., 2017; Wu et al., 2016). From space, at this stage, it is not clear how much complementary measurements that help characterizing the light path in the presence of optically thin clouds and aerosols (e.g., Bertaux et al., 2020; Rusli et al., 2020) or variations in the observation local time can increase the data yield in key emission regions. In addition, the modest

XCO_2 signal suggested by our model simulation (usually smaller than the retrieval random errors) in most areas affected by the pandemic suggests the importance of demonstrating a sufficient metrological resolution for averages of retrievals, possibly with direct (in situ) measurements of XCO_2 (Karion et al., 2010), so that small variations of XCO_2 can be robustly characterized.

Data Availability Statement

OMI data version 3 were obtained online (https://aura.gesdisc.eosdis.nasa.gov/data/Aura_OMI_Level2/OMNO2.003/).

TROPOMI offline data versions 1.2.2 and 1.3.2 were obtained online (https://s5phub.copernicus.eu/). Mass fluxes for the LMDz simulation (http://dods.lsce.ipsl.fr/invsat/LMDZ/) have been generated by Marine Remaud. Carbonmonitor data are available online (https://carbonmonitor.org/).

Acknowledgments
The present work was granted access to the HPC resources of TGCC under the allocation A0070102201. OCO-2 retrievals were produced by the OCO-2 project at the Jet Propulsion Laboratory, California Institute of Technology and obtained from the OCO-2 data archive maintained at the NASA Goddard Earth Science Data and Information Services Center (https://disc.gsfc.nasa.gov/). David Crisp and two anonymous reviewers provided useful comments on an earlier version of the text.

References

Bertaux, J.-L., Hauchecorne, A., Lefèvre, F., Bréon, F.-M., Blanot, L., Jouglet, D., et al. (2020). The use of the 1.27μm O_2 absorption band for greenhouse gas monitoring from space and application to MicroCarb. *Atmospheric Measurement Techniques*, *13*, 3329–3374. https://doi.org/10.5194/amt-13-3329-2020

Broquet, G., Bréon, F.-M., Renault, E., Buchwitz, M., Reuter, M., Bovensmann, H., et al. (2018). The potential of satellite spectro-imagery for monitoring CO_2 emissions from large cities. *Atmospheric Measurement Techniques*, *11*, 681–708. https://doi.org/10.5194/amt-11-681-2018

Carbonmonitor (2020). https://carbonmonitor.org/, last access: 17 June 2020

Chevallier, F., Engelen, R. J., & Peylin, P. (2005). The contribution of AIRS data to the estimation of CO_2 sources and sinks. *Geophysical Research Letters*, *32*, L23801. https://doi.org/10.1029/2005GL024229

Ciais, P., Wang, Y., Andrew, R., Bréon, F.-M., Chevallier, F., Broquet, G., et al. (2020). Biofuel burning and human respiration bias on satellite estimates of fossil fuel CO_2 emissions. *Environmental Research Letters*, *15*. https://doi.org/10.1088/1748-9326/ab7835

Clery, D. (2019). Europe to lead in monitoring carbon from space. *Science*, *366*, 1176–1177. https://doi.org/10.1126/science.366.6470.1176

Eldering, A., Wennberg, P. O., Crisp, D., Schimel, D. S., Gunson, M. R., Chatterjee, A., et al. (2017). The Orbiting Carbon Observatory-2 early science investigations of regional carbon dioxide fluxes. *Science*, *358*. https://doi.org/10.1126/science.aam5745

ESA (2019). Copernicus CO_2 monitoring mission requirements document, version 2.0 of 27/09/19, ESA Earth and Mission Science Division document ref. EOP-SM/3088/YM-ym, https://esamultimedia.esa.int/docs/EarthObservation/CO2M_MRD_v2.0_Issued20190927.pdf

Gurney, K. R., Liang, J., Patarasuk, R., O'Keeffe, D., Huang, J., Hutchins, M., et al. (2017). Reconciling the differences between a bottom-up and inverse-estimated $FFCO_2$ emissions estimate in a large US urban area. *Elementa: Science of the Anthropocene*, *5*, 44. https://doi.org/10.1525/elementa.137

Hersbach, H., Bell, B., Berrisford, P., Hirahara, S., Horányi, A., Muñoz-Sabater, J., et al. (2020). The ERA5 global reanalysis. *Quarterly Journal of the Royal Meteorological Society*, *146*. https://doi.org/10.1002/qj.3803

Hourdin, F., Foujols, M.-A., Codron, F., Guemas, V., Dufresne, J.-L., Bony, S., et al. (2013). Impact of the LMDZ atmospheric grid configuration on the climate and sensitivity of the IPSL-CM5A coupled model. *Climate Dynamics*, *40*, 2167–2192. https://doi.org/10.1007/s00382-012-1411-3

IPCC (2006). 2006 IPCC guidelines for National Greenhouse Gas Inventories. In H. S. Eggleston, L. Buendia, K. Miwa, T. Ngara, K. Tanabe (Eds.), *Prepared by the National Greenhouse Gas Inventories Programme*. Japan: IGES. Retrieved from https://www.ipcc-nggip.iges.or.jp/public/2006gl/index.html

IPCC (2018). Summary for policymakers. In V. Masson-Delmotte et al. (Eds.), *Global warming of 1.5°C. An IPCC Special Report on the impacts of global warming of 1.5°C above pre-industrial levels and related global greenhouse gas emission pathways, in the context of strengthening the global response to the threat of climate change, sustainable development, and efforts to eradicate poverty* (pp. 1–32). Geneva, Switzerland: World Meteorological Organization. Retrieved from https://www.ipcc.ch/site/assets/uploads/2018/10/SR15_SPM_version_stand_alone_LR.pdf

Janssens-Maenhout, G., Pinty, B., Dowell, M., Zunker, H., Andersson, E., Balsamo, G., et al. (2020). Towards an operational anthropogenic CO_2 emissions monitoring and verification support capacity. *Bulletin of the American Meteorological Society*, *101*. https://doi.org/10.1175/BAMS-D-19-0017.1

Karion, A., Sweeney, C., Tans, P., & Newberger, T. (2010). AirCore: An innovative atmospheric sampling system. *Journal of Atmospheric and Oceanic Technology*, *27*, 1839–1853. https://doi.org/10.1175/2010JTECHA1448.1

Krotkov, N. A., Lamsal, L. N., Celarier, E. A., Swartz, W. H., Marchenko, S. V., Bucsela, E. J., et al. (2017). The version 3 OMI NO2 standard product. *Atmospheric Measurement Techniques*, *10*, 3133–3149. https://doi.org/10.5194/amt-10-3133-2017

Le Quéré, C., Jackson, R. B., Jones, M. W., Smith, A. J. P., Abernethy, S., Andrew, R. M., et al. (2020). Temporary reduction in daily global CO_2 emissions during the COVID-19 forced confinement. *Nature Climate Change*, *10*(2020), 647–653. https://doi.org/10.1038/s41558-020-0797-x

Levelt, P. F., van denOord, G. H. J., Dobber, M. R., Mälkki, A., Visser, H., de Vries, J., et al. (2006). The ozone monitoring instrument. *IEEE Transactions on Geoscience and Remote Sensing*, *44*(5), 1093–1101. https://doi.org/10.1109/tgrs.2006.872333

Liu, Z., Ciais, P., Deng, Z., Lei, R., Davis, S. J., Feng, S., et al. (2020). Near-real-time monitoring of global CO_2 emissions reveals the effects of the COVID-19 pandemic. *Nature Communications*, *11*(1). https://doi.org/10.1038/s41467-020-18922-7

Myllyvirta, L. (2020). *Analysis: Coronavirus temporarily reduced China's CO_2 emissions by a quarter, 19 Feb 2020*. https://www.carbonbrief.org/analysis-coronavirus-has-temporarily-reduced-chinas-co2-emissions-by-a-quarter

Nassar, R., Hill, T. G., McLinden, C. A., Wunch, D., Jones, D. B. A., & Crisp, D. (2017). Quantifying CO_2 emissions from individual power plants from space. *Geophysical Research Letters*, *44*, 10,045–10,053. https://doi.org/10.1002/2017GL074702

Osterman, G., O'Dell, C., Eldering, A., Fisher, B., Crisp, D., Cheng, C., et al. (2020). *Orbiting Carbon Observatory-2 & 3(OCO-2 & OCO-3)—Data product user's guide, operational level 2 data versions 10 and lite file version 10 and VEarly. Version 1.0, revision A, 8 June 2020.*

Pasadena, CA: Jet Propulsion Laboratory. Retrieved from https://docserver.gesdisc.eosdis.nasa.gov/public/project/OCO/OCO2_OCO3_B10_DUG.pdf

Pinty, B., Janssens-Maenhout, G., Dowell, M., Zunker, H., Brunhes, T., Ciais, P., et al. (2017). *An operational anthropogenic CO_2 emissions monitoring & verification support capacity—Baseline requirements, model components and functional architecture*. Brussels, Belgium: Commission Joint Research Centre, European Commission, Directorate-General for Communication Publications. https://doi.org/10.2760/39384

Remaud, M., Chevallier, F., Cozic, A., Lin, X., & Bousquet, P. (2018). On the impact of recent developments of the LMDz atmospheric general circulation model on the simulation of CO_2 transport. *Geoscientific Model Development*, *11*, 4489–4513. https://doi.org/10.5194/gmd-11-4489-2018

Reuter, M., Buchwitz, M., Schneising, O., Krautwurst, S., O'Dell, C. W., Richter, A., et al. (2019). Towards monitoring localized CO_2 emissions from space: Co-located regional CO_2 and NO_2 enhancements observed by the OCO-2 and S5P satellites. *Atmospheric Chemistry and Physics*, *19*, 9371–9383. https://doi.org/10.5194/acp-19-9371-2019

Rusli, S. P., Hasekamp, O., aan de Brugh, J., Fu, G., Meijer, Y., & Landgraf, J. (2020). Anthropogenic CO_2 monitoring satellite mission: The need for multi-angle polarimetric observations. *Atmospheric Measurement Techniques*. https://doi.org/10.5194/amt-2020-152

Tollefson, J. (2020). How the coronavirus pandemic slashed carbon emissions—In five graphs. *Nature*, *582*, 158–159. https://doi.org/10.1038/d41586-020-01497-0

van Geffen, J. H. G. M., Eskes, H. J., Boersma, K. F., Maasakkers, J. D., & Veefkind, J. P. (2019). TROPOMI ATBD of the total and tropospheric NO_2 data products, Report S5P-KNMI-L2-0005-RP, version 1.4.0, KNMI, De Bilt, the Netherlands, available at: http://www.tropomi.eu/documents/atbd/ (last access: 4 September 2020).

Veefkind, J. P., Aben, I., McMullan, K., Föorster, H., deVries, J., Otter, G., et al. (2012). TROPOMI on the ESA Sentinel-5 precursor: A GMES mission for global observations of the atmospheric composition for climate, air quality and ozone layer applications. *Remote Sensing of Environment*, *120*, 70–83. https://doi.org/10.1016/j.rse.2011.09.027

Warren, S. G., Eastman, R., & Hahn, C. J. (2015). Clouds and fog: Climatology. In J. Pyle & F. Zhang (Eds.), *Encyclopedia of atmospheric sciences* (2nd ed., pp. 161–169). Cambridge, MA: Elsevier. https://doi.org/10.1016/B978-0-12-382225-3.00113-4

Wu, L., Broquet, G., Ciais, P., Bellassen, V., Vogel, F., Chevallier, F., et al. (2016). What would dense atmospheric observation networks bring to the quantification of city CO_2 emissions? *Atmospheric Chemistry and Physics*, *16*, 7743–7771. https://doi.org/10.5194/acp-16-7743-2016

Zheng, B., Chevallier, F., Ciais, P., Broquet, G., Wang, Y., Lian, J., & Zhao, Y. (2020). Observing carbon dioxide emissions over China's cities and industrial areas with the Orbiting Carbon Observatory-2. *Atmospheric Chemistry and Physics*, *20*, 8501–8510. https://doi.org/10.5194/acp-20-8501-2020

Zheng, B., Geng, G., Ciais, P., Davis, S. J., Martin, R. V., Meng, J., et al. (2020). Satellite-based estimates of decline and rebound in China's CO_2 emissions during COVID-19 pandemic. *Science Advances*, *6*, eabd4998. Retrieved from https://arxiv.org/abs/2006.08196